Structural reliability analysis of a submerged floating tunnel under copula-based traffic load simulations

Torres-Alves, G. A.; 't Hart, C. M.P.; Morales-Nápoles, O.; Jonkman, S. N.

DOI
10.1016/j.engstruct.2022.114752

Publication date
2022

Document Version
Final published version

Published in
Engineering Structures

Citation (APA)
Torres-Alves, G. A., 't Hart, C. M. P., Morales-Nápoles, O., & Jonkman, S. N. (2022). Structural reliability analysis of a submerged floating tunnel under copula-based traffic load simulations. *Engineering Structures*, *269*, Article 114752. https://doi.org/10.1016/j.engstruct.2022.114752

Engineering Structures 269 (2022) 114752

Contents lists available at ScienceDirect

Engineering Structures

journal homepage: www.elsevier.com/locate/engstruct

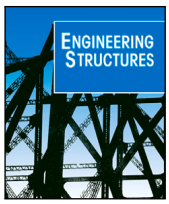

Structural reliability analysis of a submerged floating tunnel under copula-based traffic load simulations

G.A. Torres-Alves [a], C.M.P. 't Hart [a,b,c,*], O. Morales-Nápoles [a], S.N. Jonkman [a]

[a] Civil Engineering and Geosciences, Delft University of Technology, The Netherlands
[b] Royal HaskoningDHV, Amersfoort, The Netherlands
[c] Tunnel Engineering Consultants (TEC), Amersfoort, The Netherlands

ARTICLE INFO

Keywords:
Submerged floating tunnel
Reliability
Probability
Bending moments
Copula
Traffic
Direct stiffness method
Differential equation method

ABSTRACT

A submerged floating tunnel (SFT) is a structure that has been proposed as an innovative solution for waterway crossings around the world. However, to this day, no SFT has been constructed yet. One of the main reasons is that there is an insufficient insight into the structural reliability of the SFT. Here, a method to assess the expected structural response of an SFT under traffic loads and a reliability assessment of the results is presented. To do this, traffic models and structural response and reliability are coupled. The methodology presented herein proposes an innovative way to combine copula-based models and structural models to obtain more a more realistic structural response of the SFT. The focus will be on one failure mechanism, leakage caused by bending failure of the SFT in the longitudinal direction. The method utilizes a copula-based model to characterize the traffic loads and simulate traffic loads on the SFT (axle weight, inter-axle distance, and inter-vehicle distance). Next, a structural model is used to assess the structural response and derive stresses. Using a probabilistic analysis, the design of the cross-section can be adapted so that it meets the requirements for leakage caused by bending moments. For the case study is demonstrated that for a buoyancy weight ratio (BWR) of 1.1 an optimal design can be achieved based on a probabilistic method. This methodology could be extended to other failure modes of an SFT or to other structures.

1. Introduction

A submerged floating tunnel (SFT) or also known as Archimedes' bridge is a tubular structure submerged in water at a fixed depth, which exploits the bearing capability offered by the Archimedes buoyancy [1]. Tethered SFTs are stabilized on their position by anchorage systems made of cables attached to the seabed, while pontoon SFTs use floating pontoons on the free water surface [2] (Fig. 1). First proposals appeared in the early decades of 1900 in Norway, however, just in the last years several preliminary designs and feasibility studies have been proposed [2]. Nevertheless, no SFT has been constructed yet. One of the reasons for this is the lack of experience and research regarding possible SFT's structural responses to different load actions and there is no insight in its safety or structural reliability. Since an SFT is situated in a marine environment, the loads on an SFT can be divided into environmental loads, permanent loads, operational loads, deformation loads, and accidental loads [3].

The effect of the aforementioned loads on the structure can be very complex [3]. Generally, the reliability assessment of structures is carried out by applying variables as deterministic values. Moreover, insight is required in the structural reliability and risk levels associated with a certain design and loading conditions. An SFT is similar to an immersed tunnel (IMT). For example, both depend on gravity-induced vertical loads such as dead weight, vehicle weight, the self-weight of the structure and its buoyancy. However, an IMT is supported on the seabed, while an SFT is floating. This makes an SFT a structure in a dynamic hydraulic environment and will thus be differently (externally) loaded than an IMT. An IMT is usually covered with a protection layer of soil and continuously supported by soil bedding. An SFT structure is floating during its lifetime and relies on the balance between the up and down-ward vertical forces and is discretely supported along the alignment by pontoons or tethers. The response of an SFT is more sensitive to loading than an IMT because Flooding of an IMT will introduce a larger vertical downward force. This is a severe situation that could lead to loss of the tunnel due to the disrupted balance between the weights and the buoyancy and may lead to undesired settlements. Additionally, flooding of the hinterland might be a consequence if the hinterland's elevation is lower than the tunnel's entrance [4]. Flooding of an IMT causes considerable damage, but it might still be possible to repair

* Corresponding author at: Civil Engineering and Geosciences, Delft University of Technology, The Netherlands.
E-mail address: c.m.p.thart@tudelft.nl (C.M.P. 't Hart).

https://doi.org/10.1016/j.engstruct.2022.114752
Received 17 March 2021; Received in revised form 19 September 2021; Accepted 25 July 2022
Available online 19 August 2022

Nomenclature

$[R_{BWR}]$	Matrix of results due to the BWR
$[R_e]$	Matrix of enveloped results
$[R_t]$	Matrix of results due to BWR and traffic loads
σ_f	Stress in fiber
$\vec{F}_t$	Vector of a sub-train of axle loads
a	Lever arm
C_{θ_X}	Auto-correlation model of order 1 for the time series of interest
F_t	Matrix of all sub-trains of axle loads
$G_1(x_1)$, $G_2(x_2)$	Marginal distributions
h	Cross-section thickness - Eurocode definition
$H_{X_1Y_2}$	Joint distribution
i	Discrete time indices of the variable of interest (Not calendar time) [h].
I_z	Second moment of area
M	Total bending moment.
M_{BWR}	Bending moment due to BWR load
M_{cap}	Bending moment capacity
$M_{max,min}$	Maximum or minimum bending moment from envelope
M_{pt}	Bending moment due to asymmetric post tensioning
$M_{tr,cap}$	Bending moment capacity related to traffic
M_{tr}	Bending moment due to traffic load
$N_{as,pt}$	Asymmetric post tensioning
$N_{ax,pt}$	Axial post tensioning
R_i	Inner radius of tubular section
R_o	Outer radius of section
R_u	Matrix of results for each unit load
S_{i-1}	Vehicle's speed at time $t-1$ [km/h]
t_s	Thickness of the tubular shape
w_f	Section modulus for fiber location
x_{fi}	Location of fiber in the cross-section
x_f	Vertical location of fiber
x_i	Inter-vehicle distance at discrete time t [km]
ecdf	Empirical cumulative distribution function.

after pumping out the water, cleaning the tunnel and repair of the tunnel installations. When an SFT is flooded, it could also lead to loss of the structure [5]. A tether-type SFT [6] is particularly vulnerable to total destruction by flooding. However, according to Grantz (2010) [6], pontoon-type SFT structures are also vulnerable to total destruction by flooding.

An SFT will be subject to several different loads over time, such as wind and wave loads, collisions risk, tidal loads, and internal loads. Together with these loads, also other failure mechanisms can be considered. The method presented in this paper is based on a hypothetical single tube tunnel with an outer radius of 5 m, a wall thickness of 1 m, and spans of equal size of 200 m. The focus is on the relation between traffic load over time and the resistance to leaking due to cross-sectional failure. Although intentions to build an SFT exist for decades already an SFT have never been built yet, but a first design guide for SFT structures was published recently [7]. This guide describes several other design and loading situations than the one considered in this paper. The method here presented focuses on failure due to bending caused by traffic, other loads and failure mechanisms are beyond the scope of this paper.

In this paper, a pontoon-type SFT (Fig. 1) is presented as a case study. This SFT is tested for traffic loads and its structural response is investigated to assess its reliability. The traffic load is defined as a fluctuating load both in magnitude as in occurrence and position over the structure. A traffic model based on WIM (Weight in motion) data of heavy vehicles (heavier than 3.5 tons) is used to represent traffic at the tunnel. In a pontoon-type SFT, the weight loads are larger than the buoyancy load of the structure and the traffic loads act in the same vertical downward direction as the resulting forces of the permanent loads. Thus, the traffic loads will add to the resulting forces caused by the permanent and buoyancy loads. An SFT must have sufficient reserve capacity to be able to carry the traffic load [8]. On the other hand, in a tethered-type SFT, the permanent loads act in the opposite direction. The traffic loads and resulting forces of the permanent loads compensate each other.

The methodology presented in this paper is based on probabilistic modeling (copula-based models) of the input parameters, mathematical calculation methods, and structural design principles. Our approach results in a more realistic approximation of the structural response of the SFT. The SFT is tested for one failure mechanism: leakage failure due to longitudinal bending of the SFT tube. Roughly, this methodology consist of (i) simulating the traffic passing through the SFT using a copula-based model where WIM data is the input, (ii) computing the resulting bending moments, shear forces and displacements of the SFT through a finite element method (FEM) model, and (iii) performing a reliability analysis on the bending moments obtained in the previous step. More details of this methodology are presented in the next section.

Traditionally, the requirements on structures are based on the target reliability which is related to the consequences. The target reliability requirements increase if the consequences become larger. The discussion about the target reliability on structures is diverse and for SFT structures, Several standards define a target reliability for different types of structures based on the consequences, for example [9,10]. These standards use a semi-probabilistic approach using a Load Resistance Factor Method (LRFM). Other, more sophisticated and complex, are used to calibrate the LRFM. A calibration of LRFM for tunnels sections has been conducted in [11,12]. Different approaches for risk and reliability, semi-probabilistic, reliability based and risk informed, are described in [13,14]. SFT structures have not been built yet and the discussion about the required target reliability for SFT is ongoing. Both [15,16] contribute to this discussion. This paper presents a design adaption related to uncertainty and less predictable loading over time that is independent to the required target reliability. The relation of this method to other reliability methods is beyond the scope of this paper, such is described in [13,14]. The method presented in this paper results in a reliability in terms of return period for a design. If the reliability requirement is not met, the design need to be adapted.

A similar approach as the one presented here was used for investigating bridges under traffic and earthquake loads in [17], where only heavy vehicles are investigated. The methodology presented in [18] uses empirical copulas to characterize WIM data to assess the load effect of heavy trucks on bridges. Copula models have been used in the past in transportation studies. Spissu et al. (2009) [19] proposed a copula-based model to study the relationship between vehicle type choice and usage (miles traveled). While in [20] the effects on travel behavior are analyzed by studying the dependence between residential neighborhood choice and daily household vehicle miles per travel (VMT). In relation to traffic variables, Zou & Zhang (2016) [21] used a copula-based model to characterize the dependence between vehicle speed, headway and length.

Other variables such as corrosion growth have been characterized using copulas for the assessment of steel girder bridges [22]. Modeling of environmental loads are also a topic of interest for the assessment of structures, for example, in [23], a copula-model is used to characterize

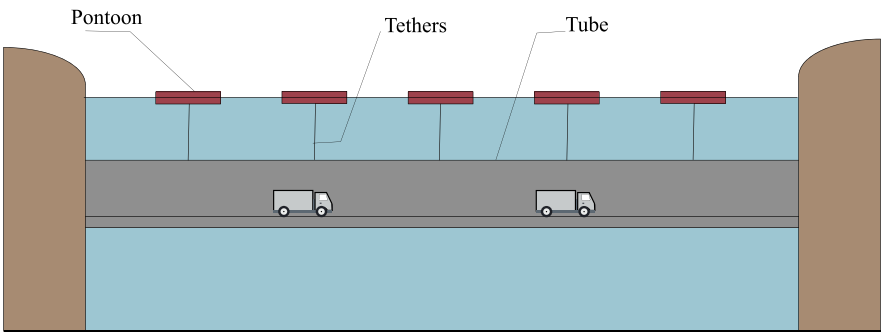

Fig. 1. Pontoon-type SFT.

the joint distribution of wind speed and rain intensity to perform a failure analysis of a transmission line. In [24], wind speed and air temperature are characterized using copulas for the assessment of long span bridges. Another example of an application of copula-based models and reliability analysis was presented in [25] to investigating the failure of a dike by overflow.

Engineers, researchers and decision-makers can benefit from this study to better understand the SFT response to traffic loads. The flexibility of this methodology also allows to study different configurations of SFT (tethered or supported by underwater piers). Moreover, this methodology can be applied to other variables of interest that may affect the structure under investigation, such as metocean loads (waves and currents), among others. Finally, this work can be used as a reference when data is scarce since copula models can produce simulations that retain the probabilistic dependence between the variables.

This paper starts by describing the methodology to perform the load simulation, structural model, and reliability analysis. Next, a brief description of the data-set is presented. After the data description, the application of the model to the case study is presented. Finally, a discussion, conclusions, and recommendations for future research are presented.

2. Modeling approach

2.1. General overview

In this section, the methodology to perform a reliability analysis of an SFT using a combination of copula-based models and structural FEM models is presented. The reliability analysis is conducted by the definition of the Limit State Function. An SFT structure is a buoyant structure where leakage will cause unbalance of the structure and could initiate a progressive collapse. In this paper, the limit state function is based on leakage caused by bending moments as a result of traffic loads. SFT structures can be affected by different types of loads and leakage due to bending failure is just one of the many failure modes. However, other failure modes or the influence of other loading variables are considered beyond the scope of this research. The modeling approach employed in this paper consists of the following steps (Fig. 2):

- First, simulation of traffic passing through the SFT is carried out by using a copula-based model that characterizes the distance between vehicles (also known as inter-vehicle distance).
- Simulation of traffic is carried out for a determined "period of time" based on an average number of vehicles per unit time (i.e. one year). The result is a "train" of vehicles that will include, number of axles, axle weights, inter-axle distances, and inter-vehicle distances.
- Then, the resulting time series of traffic are used as input in a FEM model, based on the Direct Stiffness Method (DSM) and the Differential Equation Method (DEM), to test its effect on the structure of the SFT in terms of cross-section results, like bending moments, shear forces, and displacements.
- From the bending moments, a stress distribution can be derived in order to validate the compression zone of the section.
- Finally, a reliability assessment is performed on the limit state (leakage failure mechanism due to bending moments in the longitudinal direction). Findings on the assessment can lead to adjustment or optimization of the water-tightness of the SFT section.

2.2. Copulas for inter-vehicle distance

The traffic load passing through the tunnel is defined by four main variables (Fig. 3), (i) Axle weight ($AX1, AX2$), (ii) inter-axle distance ($DTF1, DT12, DTLAE$), (iii) inter-vehicle distance (X_t), and (iv) number of axles per vehicle. In this paper, a copula-based model is used to characterize the inter-vehicle distance by estimating the auto-correlation of this variable. This allows us to create a more realistic modeling of the traffic passing through the SFT. Distinction between inside and outside congestion hours are also considered for this analysis.

A bi-variate copula, or simply a copula for the purposes of this paper, is a joint distribution with uniform margins in [0,1]. Sklar's theorem [26] states that any multivariate joint distribution can be written in terms of the uni-variate marginal distribution functions and a copula that describes the dependence between the random variables. For the bi-variate case:

$$H(x_1, x_2) = C\{G_1(x_1), G_2(x_2)\} \tag{1}$$

Here, $H\left(x_1, x_2\right)$ is the joint distribution of the two continuous random variables (X_1, X_2) with marginal distribution $G_{X_1}(x_1)$ and $G_{X_2}(x_2)$ in the interval $[0, 1]$ and a copula taking values from the unit square $I^2 = ([0, 1] \times [0, 1])$, such that for all (x_1, x_2) Eq. (1) is satisfied. If G_{X_1} and G_{X_2} are continuous, then C is unique. For a complete treatment of copula modeling the reader is referred to [27] and references therein.

In order to estimate the parameters, select the model and simulate the bi-variate copula models, the VineCopula package [28] is used. This tool is developed in R, a free software environment for statistical computing and graphics [29]. The package includes copulas such as Gaussian, Gumbel, Clayton, t, Joe, BB1, BB6, BB7, BB8, as well as their rotated versions. The parameters are estimated by pseudo maximum likelihood and the copula families were selected based on Akaike's information criterion (AIC).

Let X denote a random variable (i.e. the inter-vehicle distance) with distribution G_X. The time series of interest is $\{X_t\}, t \in \mathbb{N}$. The transition distribution is given by Eq. (2).

$$H(x_t|x_{t-l}) = P(X_t \leq x_t|X_{t-1} = x_{t-1}) = C_{\theta_X}\left(G(x_t)|G(x_{t-1})\right) \tag{2}$$

where $C_{\theta_X}(u|v)$ is the conditional copula. Notice that the parameter θ_X would model auto-correlation of order 1 for the time series of interest. In this study, for a sequence of inter-vehicular distance, the formulation in Eq. (2) is used to simulate values for the distance between vehicles.

The graphical representation of this process is presented in Fig. 4.

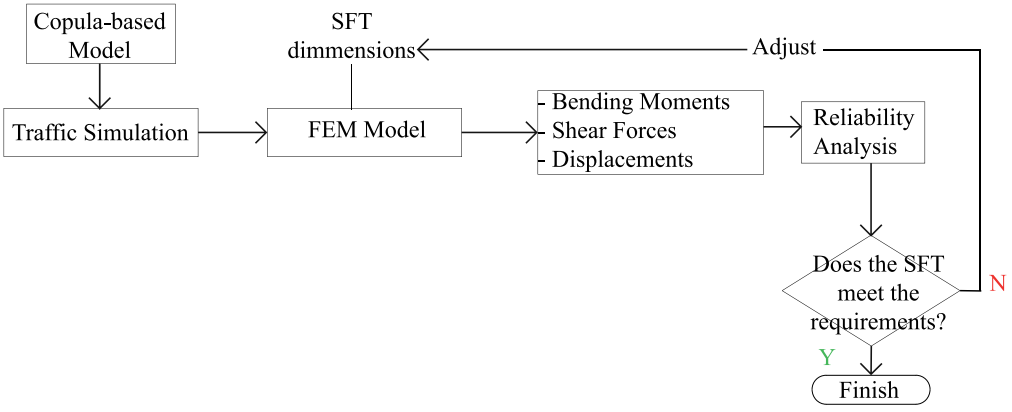

Fig. 2. Modeling overview flowchart.

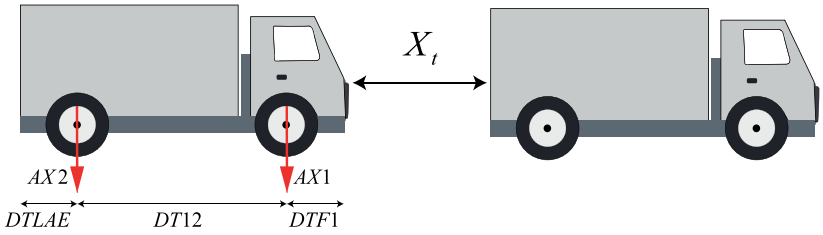

Fig. 3. Traffic variables.

$$\ldots \quad X_{t-1} \longrightarrow X_t \longrightarrow X_{t+1} \quad \ldots$$

Fig. 4. Graphical representation of the process for inter-vehicle distance.

This model has been proposed before in [30,31] for traffic loads modeling in bridge reliability and for modeling time series of hydrological variables in [25].

2.3. Simulating traffic

An algorithm was developed to simulate traffic through the SFT. The main goal of this algorithm is to capture the daily characteristics of different traffic scenarios while maintaining the proportion of vehicle per traffic scenario and category.

The simulation consists of 4 main steps, (i) simulating the number of vehicles (per day, lane, traffic scenario and vehicle category), (ii) simulation of inter-vehicle distances (X_t) using a copula-based model (per traffic scenario), (iii) random sampling of axle weights and respective inter-axle distances from a vehicle data base (VH) and, (iv) combining the results from the previous steps to form a "train" of vehicles.

The algorithm starts by loading the required variables and the fitted copulas corresponding to each traffic scenario. The simulation is performed daily, where the number of vehicles per lane is randomly sampled from its corresponding empirical cumulative distribution function (ecdf). Then, the number of vehicles per traffic scenario and category is obtained by multiplying the total number of vehicles per lane by its corresponding vehicle proportion. This operation is carried out until the desired number of days to simulate is reached.

Next, for each traffic type, the simulation of inter-vehicle distances is executed from its corresponding fitted copula. And, since the vehicle category proportion per traffic type is known, the random extraction of axle-weights and inter-axle distances from the VH data-set is carried out.

Finally, the inter-vehicle distances (X_t), axle-weights and inter-axle distances are put together in a vector to form a "train" of vehicles (Fig. 3) that is used as input for the structural model. A simplified flowchart of the traffic simulation algorithm can be found in Appendix A.

2.4. Structural model

In this paper, the structural system of the SFT is characterized by beams supported by pontoons. The methodology for the structural model is based on the Direct Stiffness Method (DSM) and the Differential Equation Method (DEM). This methodology is used to analyze the structure and to determine the structural response in terms of cross-section results, such as bending moments. The application of these methods is focused on computational efficiency. The selected structural system of beams which suffices for this analysis. However if the structure is loaded by 3 dimensional and dynamic loading, like wave loads, impact load and others, a different modeling approach is required, using shell or solid models.

With this slender implementation, the same geometrical model can be used for multiple load cases with arbitrarily located discrete loads without the need to split the model into many elements. In this way, a performance penalty is avoided.

2.5. SFT structure

In this section, a brief description of the SFT's structure, its dimensions, loading representation and structural response is presented. The SFT model has spans of equal size (200 m) and the tethers' stiffness is the same for all pontoon connections. The pontoons by themselves are considered as hinged supports. A graphical representation of this model is presented in Fig. 5. The model is simplified by considering only 2 full spans and 2 half side spans with symmetry supports (fixed rotations, free vertical translations). The system has a total length of 600 m and is contemplated as a monolithic structure without flexible joints or hinges. In total, the structural system is built up out of 8 nodes and 7 beams.

The system is loaded with traffic loads representing the axle weights of vehicles driving through the SFT. These traffic loads are the result

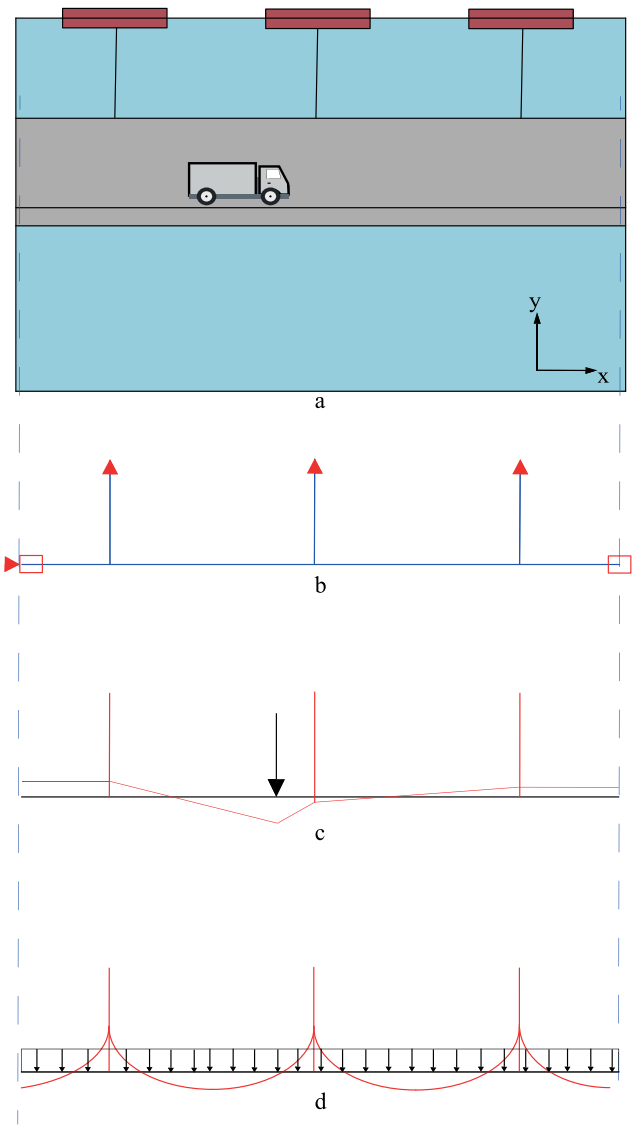

Fig. 5. From top to bottom: (a) SFT scheme, (b) Structural system, (c) Bending moments due to a unit force load, (d) Bending moments due to buoyancy weight ratio (BWR) load.

of the methodology presented in Section 2.2. The loading is defined as axles with an intermediate distance (inter-vehicle distance). Further details about the characterization of the loading is addressed in Sections 3 and 4.

Since the load represents the axles of moving vehicles, the single axle load can therefore be positioned anywhere on the structure. For this reason, a grid is defined throughout the structure with a grid size of 1 m, resulting in a total of 600 individual positions along the structure. For each of the 600 individual positions an unified axle load can be used to calculate the individual influence on the system cross-sections results (bending moments, shear forces) as presented in Fig. 5b and c.

Commonly, in global design analyses, linear structural behavior is used to find the global response of the structure. Non-linear effects such as cracking or plasticity are considered in local cross-sectional analyses to design reinforcement or validation of the section. In this paper, leakage of the SFT is considered as the limit state function. For simplicity, un-factored loads are considered. Partial load factors could be applied, but they will differ for different standards and different scenarios.

Due to the assumption of elastic response of the global structure, the superposition principle can be used. Therefore, a discrete unit load is applied on each grid point along the structure to gather the results of a single point load, resulting in 600 individual unit load cases. These cross-section results and displacements of each unit load case are gathered in matrix R_u representing a point load in each point on the grid along the SFT model. Then, this resulting matrix is multiplied by each vector sub-train of vehicles $\vec{F}_t$ using the superposition principle, which contains the factors related to the axle weight.

In this way, the axle loads can be acting in any of the 600 grid points and if for each situation a FEM analysis was conducted the analysis time would increase significantly. For each situation the unit loads are the multiplied by factors based on the axle weights and can be considered as the axle loads. The sum of all axle loads for the situation leads to the cross-sectional results for the situation.

The structural response due to each situation is obtained and added to the response caused by the BWR (R_{BWR}), as presented in Eq. (3). By applying the sub-train vector $\vec{F}_t$, the loads on the end-fields are excluded from the vector $\vec{F}_t$ due to symmetry. This symmetry acts as a mirror for the loads over the support condition. A single load on an end-field will then be considered as a double load but mirrored over the support condition. The envelope of all situations including the results from the BWR will present the maximum cross-sectional forces.

For the case of a pontoon-SFT, the total bending moments are the result of the upward buoyancy force and the permanent loads

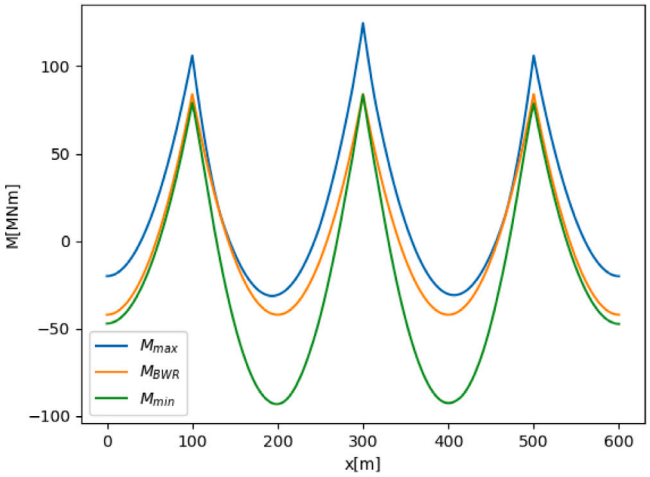

Fig. 6. Envelope of bending moments.

acting on the structure (self-weight and dead weight). The relationship between the permanent loads and the buoyancy load is described as the Buoyancy Weight Ratio (BWR) and can be influenced by changing the ballast of the structure. The resulting distributed force (BWR load) has a downward direction that coincides with the traffic loading. For simplicity, the BWR is considered constant over the length of the system. For example, for a BWR of 1.1, the permanent load acting on the structure is 10% higher than the upward buoyancy force. The bending moments caused by the BWR are presented in Fig. 5d.

The axle loads (or axle weights) and their corresponding inter-vehicle distance are treated as a long train of axle loads. Each axle load has a different magnitude. "Sub-trains" (situations, smaller portions of the train of axle loads) can be derived by moving the 600 m model over the train of vehicles. All the "sub-trains" of loads are combined in a matrix F_t on a grid position. However, the amount of sub-trains ($\vec{F}_t$) is substantial and using the DSM and DEM for each sub-train leads to a large time-consuming process.

$$[R_t] = [R_u] \cdot \vec{F}_t + [R_{BWR}] \tag{3}$$

From the cross-section results and displacements for each sub-train in (R_t), the envelope of the results (R_e) is found. Minimum and maximum values of the results, like bending moments and shear forces, can be distinguished along the structure. The resulting envelopes of the bending moments and shear forces are presented in Figs. 6 and 7. If the traffic model (Section 2.2) generates a longer data-set, then different distributions for R_e are found. For each data-set generated by the traffic model, a different R_e is found.

2.6. Limit state

The cross-section of an SFT can be of different shapes, in this paper, a tubular cross-section is used (Fig. 8). This cross-section could be (asymmetrically) post-tensioned if needed. One of the main threats of an SFT is large ingress of water (leakage). This could lead to changes in the BWR. Should this be the case, the loads acting on the structure will be larger i.e., the structure becomes heavier due to the presence of water. As a consequence, the distributed load (q_{BWR}) and R_{BWR} will increase significantly. Consequently, the design might fail to meet the requirements in terms of bending moments, forces and displacements. In a worst-case scenario, this may even cause a progressive collapse of the SFT, because leakage can lead to the appearance of other failure mechanisms (whose investigation are out of the scope of this paper).

Concrete is considered to be watertight when it is in compression, thus, tensile stresses could lead to cracking that could facilitate leakage. If concrete is in compression, leakage will not occur. In Eurocode 1992 [32], there are requirements for liquid retaining and containing structures which are based on liquid passing through cracks. Different classes are defined for liquid tightness. In class 2 and 3 (which are the highest requirements), it is required that cracks should not reach the full thickness of the structure. The requirement is set as a minimum compression zone in a section. For the SFT, this is the thickness of the tubular cross-section. If part of the thickness remains in compression (the compression zone), liquid tightness is assured. The minimum required value of this compression zone is the maximum of 50 mm or $0.2h$, where h is the section thickness. In other words, it is considered failure if the compression zone at the SFT's thickness of the tubular cross-section (t_s) is smaller than $0.2h$. The location of the compression zone in the full cross-section is presented in Eqs. (4), (5) and (6). If this water-tightness requirement is applied to the SFT structure (Section 4.1), the minimum compression zone of the section is defined by x_c, while the location of the fiber in the cross section (x_{fi}) is defined by the inner radius (R_i) and the compression zone. The sectional modulus (w_f) can be found by dividing the second moment of area (I_z) by the vertical location of the fiber (x_f). See Fig. 9.

$$x_c = 0.2t_s \tag{4}$$

$$x_{fi} = R_i + x_c \tag{5}$$

$$w_f = \frac{I_z}{x_f} \tag{6}$$

The pontoon-SFT is loaded with the BWR load and the traffic loads resulting in cross-sectional forces and moments as found in the resulting envelope (R_e). With these sectional forces and moments, the stress-distribution over the section can be derived. The post-tensioning will introduce a normal force ($N_{ax,pt}$) which is found by multiplying the post-tension stress times the area of the symmetric post-tension cables. If the post-tensioning at a section is applied asymmetrically (purple dots in Fig. 8), an additional bending moment (M_{pt}) is introduced as $N_{as,pt} \cdot a$. Where $N_{as,pt}$ is the post-tension stress multiplied by the area of the asymmetric post-tension cables and a is the lever arm defined as the location of the resultant of the asymmetric post-tension force ($N_{as,pt}$). When a superposition principle is used, the stress state (σ_f) in the specific fiber can be derived with Eq. (7) for the maximum bending moment from the envelope.

$$\sigma_f = \frac{M + M_{pt}}{w_f} + \frac{N_{ax,pt} + N_{as,pt}}{A_c} \tag{7}$$

where:

- σ_f : Stress at fiber

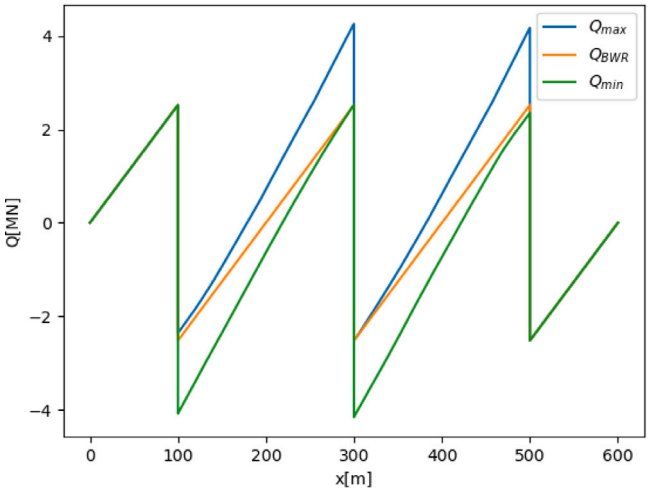

Fig. 7. Envelope of shear forces.

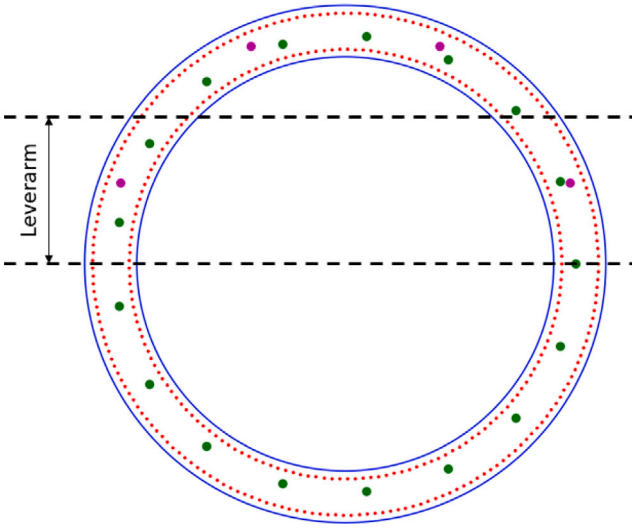

Fig. 8. Tubular section with post-tensioning and regular reinforcement (green - axial post tensioning; magenta - asymmetric post tensioning; red - regular reinforcement).

- M : Total bending moment $M = M_{tr} + M_{BWR}$
- M_{tr} : Bending moment due to traffic load envelope at the considered section
- M_{BWR} : Bending moment due to BWR load at the considered section
- M_{pt} : Bending moment due to asymmetric post tensioning defined as $N_{as,pt} \cdot a$
- $N_{ax,pt}$: Axial post tensioning
- $N_{as,pt}$: Asymmetric post tensioning
- a : Lever arm
- A_c : Section area

Analog to Eq. (3), due to the superposition principle, M_{tr} can be derived from M because M_{BWR} is a constant value for any cross-section in the model. In the limit state function, the sign conventions should be respected. Thus, M, M_{BWR} and M_{tr} will act in the opposite direction as M_{pt}. The structure fails if $\sigma_f > 0$ as shown in Fig. 9 and the SFT will suffer leakage.

Here, $\sigma_f = 0$ is considered as the limit value for the total bending moment M. Thus, the capacity for bending is defined by Eq. (8). The structure fails if M (total bending moment) is larger than M_{cap}, defined as a limit for the bending moment. Thus, the probability of failure is defined as $P_F(M > M_{cap})$. Since M_{BWR} is constant for any cross-section in the model, the limit state function for the maximum bending moment caused by traffic is Eq. (9). In that case, the structure fails if M_{tr} is larger than $M_{tr,cap}$ and the probability of failure is defined as $P_F(M_{tr} > M_{tr,cap})$.

$$M_{cap} = -N_{as,pt} \cdot a - \frac{(N_{ax,pt} + N_{as,pt}) \cdot w_f}{A_c} \tag{8}$$

$$M_{tr,cap} = -M_{BWR} - N_{as,pt} \cdot a - \frac{(N_{ax,pt} + N_{as,pt}) \cdot w_f}{A_c} \tag{9}$$

3. Traffic data and simulation

Traffic data is formed by two data-sets, namely WIM and VH. The WIM (Weight in Motion) data-set, consists of measurements of heavy vehicles at the National Highway A12 (km 42) in Woerden (The Netherlands) for two lanes (RW-12-L-2 and RW-12-L-3) [33]. These measurements include, time of measurement, vehicle category, lane, speed, the total length of the vehicle, the total weight of the vehicle, axle weight, and inter-axle distance. This data is available for 27 days in the month of April 2013 (from the 3rd to 30th) with a total of 157.000 vehicles approximately divided in 26 vehicle categories (Appendix B). All categories were considered for analysis and for traffic simulation according to their proportion within the data set. For details regarding the accuracy of the data, the reader is referred to [33]. In this data-set,

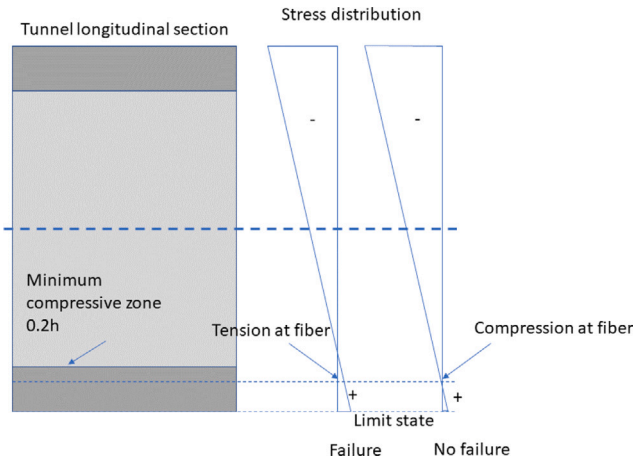

Fig. 9. Longitudinal section with respect to the limit state.

congestion was filtered automatically. In other words, measurements were neglected if the traffic had a velocity lower than 40 [km/h]. This specific WIM data-set was chosen because is used as an input for the model developed by [34] from where the second data-set (VH) is obtained (Fig. 10)

The second data-set (VH) is the result of a Bayesian Network-based (BN) model developed by [34]. The data-set is a collection of approximately 300.000 vehicles with their corresponding axle weights and inter-axle distances (that consequently define the number of axles per vehicle) that were randomly generated using the BN model. This data-set is further discussed in the next section.

For the purpose of this paper, WIM data is defined by four variables, (i) Axle weight, (ii) inter-axle distance (iii) inter-vehicle distance and, (iv) number of axles per vehicle (Fig. 3). The aim of the traffic copula-based model is the characterization of the inter-vehicle distance. In Fig. 3, X_t refers to the inter-vehicle distance (in kilometers). $AX1$, $AX2$ are the weights of axle 1 and 2 [KN]. $DTF1$, $DT12$, and $DTLAE$ are the distances between axles (in meters).

In this paper, the traffic model is focused on the characterization of the inter-vehicle distance (See Figs. 4 and 3). Nevertheless, both data-sets are used as the baseline to simulate the traffic variables that define the traffic load passing through the SFT.

3.1. Data processing

Before simulating traffic, several variables from both data-sets (WIM and VH) are combined. Moreover, there is a link between both data-sets and the copula-based model. Such a link is depicted in Fig. 10 and is discussed in the following paragraphs.

For WIM data, weekends and national holidays were excluded from the analysis. The remaining days are considered as "regular" days and were analyzed in three different time scales, hourly, daily, and monthly.

3.1.1. Hourly analysis

To study the data-set in an hourly time scale, the data-set was visualized using histograms. This allows identifying the congestion hours (hours with bigger affluence of vehicles) and free flow hours (when the number of vehicles is lower). An example is presented in Fig. 11 (April 4th), the data was classified in 3 different groups, (i) free flow before congestion hour (Free Flow A), (ii) congestion hour, and (iii) free flow after congestion hour (Free Flow B). Resulting in six different traffic scenarios: 3 groups for 2 lanes, namely, C_L2, C_L3, F_L2_A, F_L2_B, F_L3_A, and F_L3_B. Table 1 shows the meaning of this nomenclature.

Table 1
Nomenclature for hourly classification of traffic.

Nomenclature	Traffic type and lane
C_L2	Congestion lane 2
C_L3	Congestion lane 3
F_L2_A	Free flow A lane 2
F_L2_B	Free flow B lane 2
F_L3_A	Free flow A lane 3
F_L3_B	Free flow B lane 3

For these six traffic scenarios, the corresponding inter-vehicle distances $\{X_t\}$ are obtained as shown in Eq. (10) [33].

$$X_t = S_{t-1} * (i_t - i_{t-1}) \tag{10}$$

where,

- X_t: Inter-vehicle distance at discrete time t [km].
- S_{t-1}: Vehicle's speed at time $t-1$ [km/h]. It is assumed that the vehicle travels at constant speed.
- i: Discrete time indices of the variable of interest (Not calendar time) [h].

3.1.2. Daily analysis

On a daily scale, two variables are analyzed, (i) the daily distribution of vehicles per lane, and (ii) the daily proportion of vehicles per traffic scenario. Empirical cumulative distribution functions (ecdfs) are constructed to characterize the daily number of vehicles throughout the month at lane 2 and 3. This is to have insight into how the daily number of vehicles (on normal-condition days) varies. These ecdfs were not fitted to parametric distribution functions since the number of normal-conditions days is small. Consequently, the fitting would not be reliable. Fig. 11 shows that the number of vehicles in lane 2 is much smaller than in lane 3 at any time of the day. The average daily number of vehicles for lanes 2 and 3 is approximately 460 and 5150 vehicles respectively.

Regarding the daily proportion of vehicles per traffic scenario, one single day was chosen to represent the entire month. This was the result of comparing the data of every normal-condition day against each other. The criteria for choosing one day over another takes into account the daily number of vehicles and the presence of errors in the measurements. In other words, the day with the most amount of vehicles and with the least number of errors in the measurements is chosen. As a result, the 10th of April was selected as the day that will characterize this variable. Thus, the proportion of vehicles per traffic scenario was obtained from the selected day (See Appendix C). The selected proportion is used to estimate the number of vehicles per category and traffic scenario given a daily number of vehicles. The definitions of the vehicle categories are presented in Appendix B.

3.1.3. Monthly analysis

In this section, the number of vehicles per category and its corresponding proportion (%) relative to the monthly amount of vehicles was computed. The monthly proportion of vehicles is very similar to the daily proportion. This classification was applied to the entire data-set with no distinction between lanes.

The monthly proportion (Appendix D) is used as input for the BN model developed by [34] (Fig. 10). This model generates a data-set (VH) of vehicle characteristics according to its category while maintaining the same vehicle proportion as the input. In other words, the BN model provides the number of axles, axle weights, and inter-axle distances of the vehicles according to its category. For a complete overview of the BN model, the reader is referred to [34]. For this paper, the VH data-set contains 300.000 passing vehicles characterized by the category proportion presented in Appendix D.

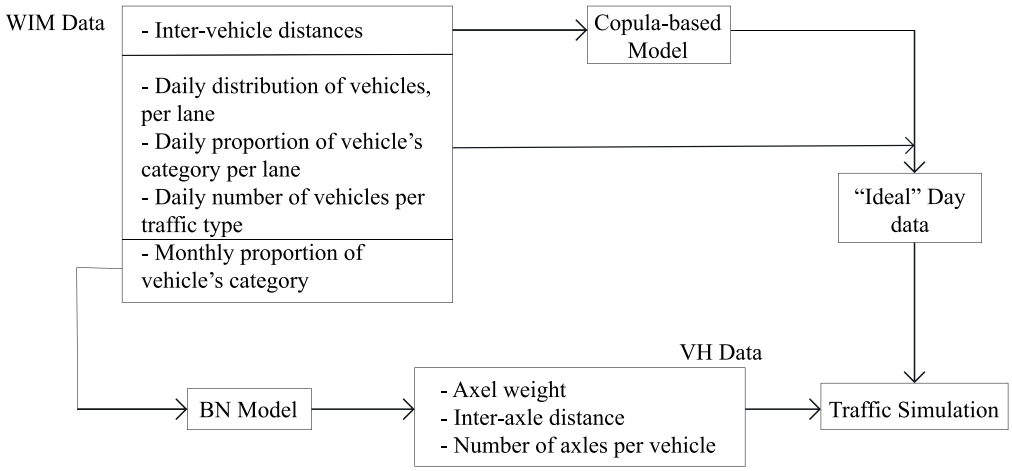

Fig. 10. Data Overview for simulation of traffic.

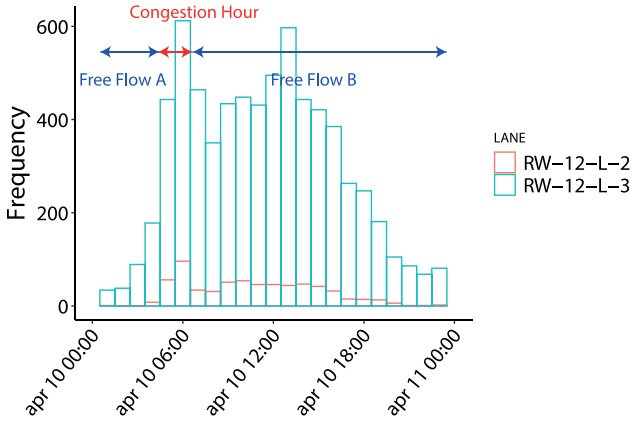

Fig. 11. Hourly classification of traffic of WIM data [33]. April 4th, 2013.

3.1.4. Creating the "ideal" day

An ideal day is defined by combining (i) the daily proportion per category and traffic type and, (ii) the fitted copulas characterizing X_t per traffic type. This ideal day is a representation of the entire month and is the basis of the traffic simulation algorithm.

As mentioned previously, the daily proportion (%) per category and traffic type is represented by data from the $10th$ of April of 2013 (Fig. 11). The inter-vehicle distances (X_t) of all traffic scenarios (of every normal-condition day) were fitted to bi-variate copulas. This process characterizes the dependence of the inter-vehicle distance and its lagged version (X_t, X_{t+1}). As a result, the auto-correlation of this variable is obtained.

Following a similar approach as for vehicle proportion, the copula that characterizes the ideal day was selected by comparing the fitted copulas (and its parameters) of every normal-condition day among the 6 traffic scenarios. The criteria for choosing an appropriate copula includes:

- The selected copula is the best fit for most of the normal-condition days of a given traffic scenario.
- The correlation value obtained from the simulated data (generated by the fitted copula) is similar to the correlation of the observations.

As a result, each traffic scenario is characterized by different copulas, each one of them belonging to different days of the month (Section 4.1).

Table 2
Selection of copula and corresponding parameters for each scenario.

Scenario	Copula	Day	Parameter 1	Parameter 2
C_L2	Gaussian	25	0.148	–
C_L3	Frank	10	−0.304	–
F_L2_A	Joe	17	1.519	–
F_L2_B	BB8	17	1.717	0.900
F_L3_A	Gumbel	17	1.137	–
F_L3_B	Joe	11	1.160	–

4. Results

4.1. Copula-based model for inter-vehicle distances

As mentioned in Section 3.1, traffic is characterized by six different traffic scenarios (Table 1). By combining the fitted copulas of each traffic scenario with the selected daily proportion of vehicles, an "ideal-day" data-set is formed. This data-set is the basis for the simulation of traffic through the SFT.

Table 2 presents the copulas that were selected for each scenario and its corresponding parameters (See Table 1 for nomenclature). Note that copulas from different days characterize each one of the traffic scenarios. The VineCopula package (in R), developed by [28] was used to fit the copulas to the data-sets (Section 2.2). The parameters were estimated by pseudo maximum likelihood and the copula families were selected based on Akaike's Information Criterion (AIC).

Table 3 shows the Spearman's correlation value for the observations (X_t, X_{t+1}). Note that the correlation values are relatively low, especially for C_L2 and C_L3. Nevertheless, the selected copulas are able to capture well the characteristics of the inter-vehicle distance for the simulation of traffic.

For the case of C_L3, the correlation value is negative. This means that the inter-vehicle distance at time t increases the inter-vehicle distance at time $t + 1$ decreases or vice versa. Physically, this means that when a vehicle gets closer to the one in front of it, it gets further away from the vehicle behind. Similarly, a positive correlation means that the inter-vehicle distance behind a vehicle increases as the distance behind it also increases.

Fig. 12 shows the simulated inter-vehicle distances together with the observations for each traffic type. The data is presented as standard normal. The plots from both simulations and observations are very similar. Notice that the observations for congestion traffic scenarios (Figs. 12(a)–12(b)) are clustered mostly in the center with their shape resembling a circle. Although the plots for the free flow scenarios (Figs. 12(c)–12(f)) are clustered in the center, they present a slight asymmetry in the upper right corner of the plots. Nevertheless, the

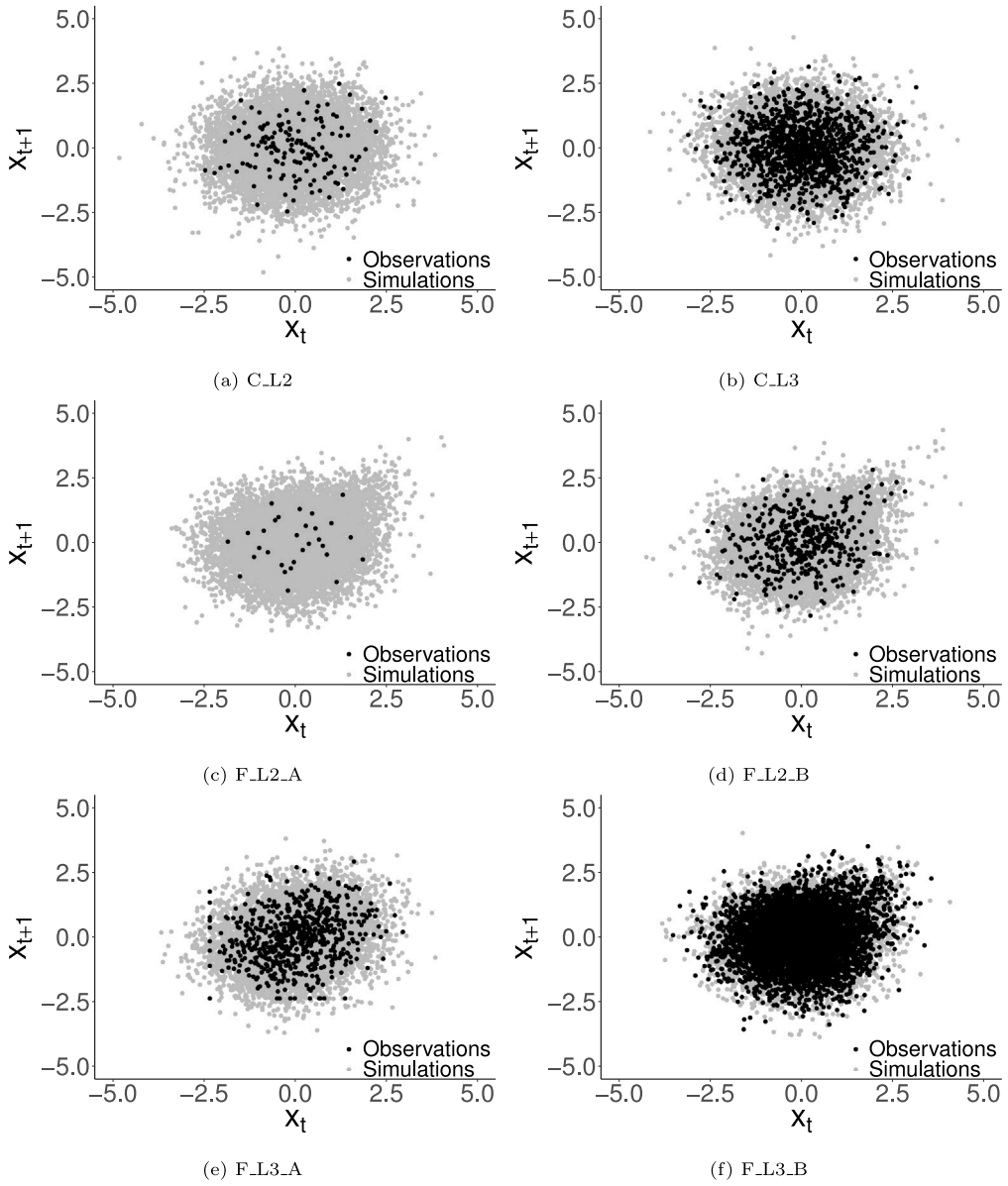

Fig. 12. Observations and simulations for inter-vehicle distances (X_i, X_{i+1}) for all traffic scenarios from (a) Gaussian Copula, (b) Frank Copula, (c) Joe Copula, (d) BB8 Copula, (e) Gumbel Copula and (f) Joe Copula; parameters are estimated via maximum likelihood. The data is presented in standard normal units.

Table 3
Spearman's Rho correlation value for observations of traffic scenarios.

	Correlation
C_L2	0.103
C_L3	−0.093
F_L2_A	0.414
F_L3_A	0.289
F_L2_B	0.054
F_L3_B	0.10

dependence structure of these copulas does not present great asymmetry and the correlation values of the observations and simulations are very similar despite of being relatively small. This is confirmed by the results presented in Appendix E. The resulting simulated traffic series has an extent of 1 year (365 days) and it represents traffic under normal conditions since weekends and national holidays were ignored in the analysis. This time series is used as input for the structural model.

4.2. Structural model

In order to derive the structural response of the SFT, a model that combines the Direct Stiffness Method (DSM) and the Differential Equation Method (DEM) is proposed. The structural model is based on an arbitrary design of a pontoon-SFT structure that contains the basic elements for a design calculation of a single tube tunnel layout. From this structure, two spans with two half adjacent spans are modeled. The tubular section has an outer radius R_o = 5 m, a wall thickness of t_s = 1 m, and a BWR of 1.1 is assumed. When the structure is loaded by a BWR of 1.1, the resulting bending moments (M_{BWR}) at the tethers and center of the span are 84 MNm and −42 MNm respectively. To ensure water tightness, 200 mm of the section needs to be in compression. For the middle section, a minimum axial compression force ($F_{ax,pt,center}$) equal to 17.2 MN is needed to ensure water tightness. For the section at the tethers, the force $F_{ax,pt,tether}$ needs to be at least 34.4 MN. Both of these forces can be accommodated by regular axial post-tensioning with equally distributed post-tension tendon around the circumferential. For tendon of 15 strands with an area of 150 mm^2 and a post-tension stress

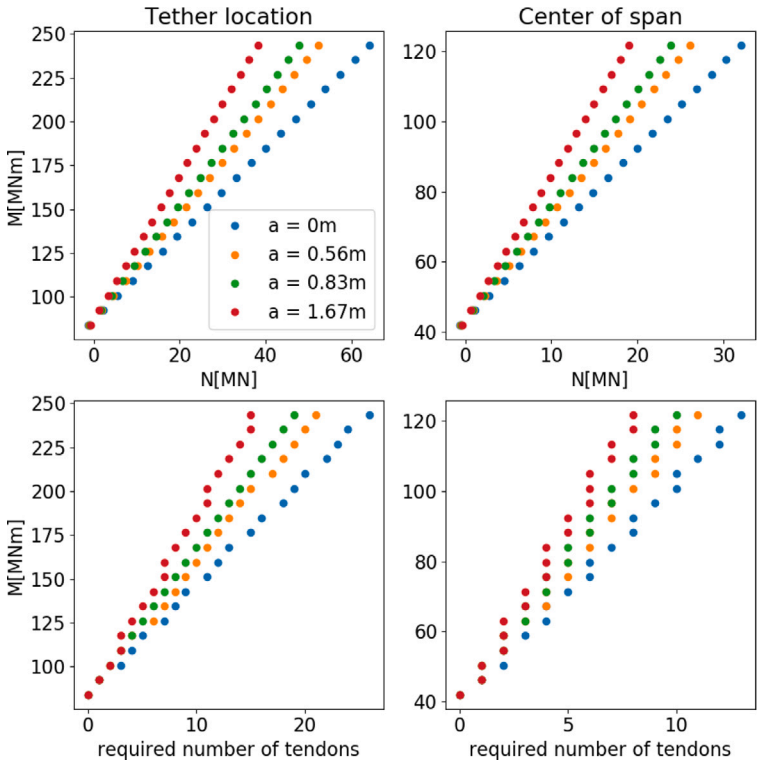

Fig. 13. Bending moments related to the required normal force and number of tendons.

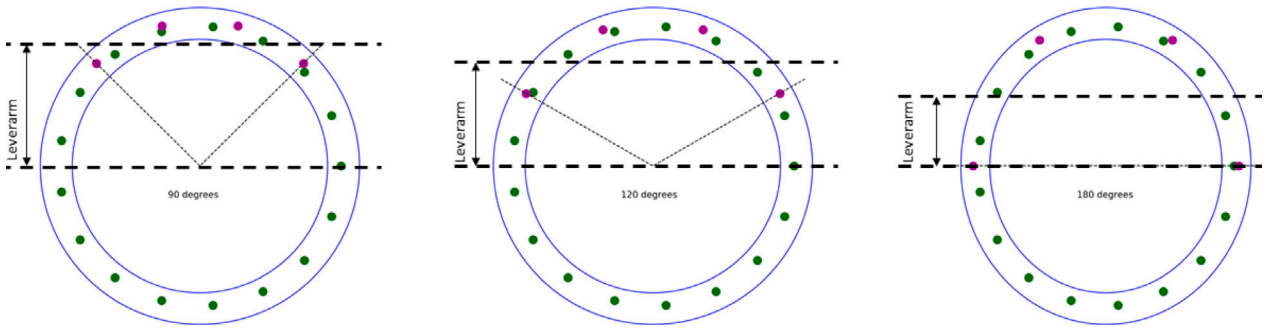

Fig. 14. Different tendon layout for 60, 120 and 180 degrees spread (purple).

Table 4
Distribution Fitting for bending moments and shear forces.

BWR	M_{max} [MNm]	M_{min} [MNm]	V_{max} [MN]	V_{min} [MN]
0	Gamma	G.E.V.[a]	Lognormal	Birn-S[b]
1.1	G.E.V.	G.E.V.	G.E.V.	G.E.V.
1.2	G.E.V.	G.E.V.	G.E.V.	G.E.V.
1.3	G.E.V.	G.E.V.	G.E.V.	G.E.V.
1.4	G.E.V.	G.E.V.	G.E.V.	G.E.V.
1.5	G.E.V.	G.E.V.	G.E.V.	G.E.V.

[a]Birnbaum–Saunders.
[b]Generalized Extreme Value Distribution.

of 950 N/mm^2, a post-tensioning force of 2.14 MN is found. Either 9 and 17 post-tension tendons will suffice for either of the both positions. In Fig. 8, the green dots represent 17 tendons that are distributed symmetrically over the circumference.

The bending moments will increase due to the action of the traffic loads as presented in Fig. 6. The design challenge is to provide post-tensioning to meet the reliability requirement of the system regarding leakage and the minimum compression zone. If the requirement is not met, additional post-tension can be applied. If additional tendons are applied asymmetrically (presented in Fig. 8 in purple), a counter balancing bending moment is introduced. This is beneficial to the capacity of the particular axial section. The amount of asymmetry can be found in the lever arm (a) of the resultant force and moment of the post-tensioning. If the lever arm (Fig. 14) is increased, the counterbalancing bending moment will be larger. Therefore, a larger lever arm will supply a larger counterbalancing bending moment with the same amount of post-tension tendons (Fig. 14) . However, the lever arm is limited by geometrical requirements such as the physical section, shape, and the minimum distance between two tendon heads. The center to center (ctc) distance between asymmetric tendons is estimated on 1 m, however, optimizing this distance to a smaller distance could improve the design but is beyond the scope for this paper. The relationship between bending moments and normal forces due to post tensioning and the number of tendons for different lever arms is presented in Fig. 13.

With the number of tendons, the normal force due to post-tensioning is found, and the bending moment is obtained by multiplying the total normal force due to post-tension by the lever arm. For simplicity, the same post-tension tendons were used in this analysis.

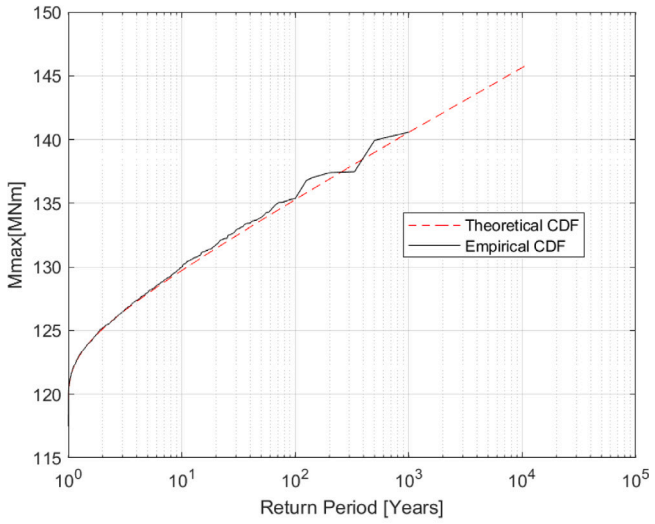

(a)

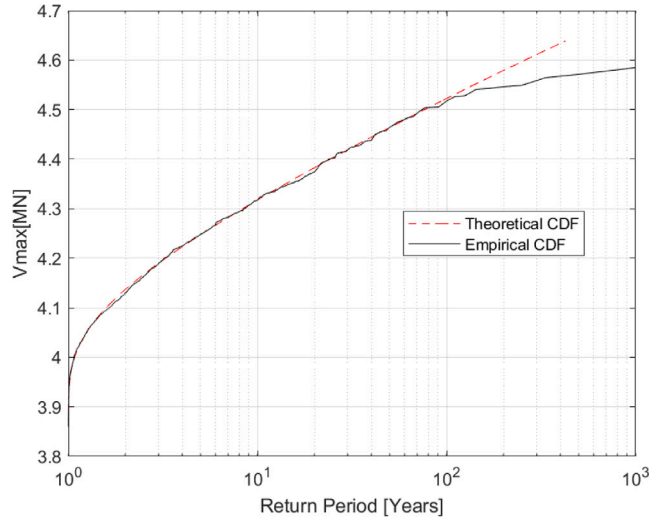

(b)

Fig. 15. Frequency curves for (a) M_{Max} [MNm] and (b) V_{Max} [MN] for a 1.1 BWR.

Table 5
Parameters of the fitted distributions.

BWR	M_{max} [MNm]			M_{min} [MNm]			V_{max} [MN]			V_{min} [MN]		
	Shape	Scale	Location	Shape	Scale	Location	Shape	Scale	Location	Shape	Scale	Location
0	25.88	0.95	–	−0.04	5.39	22.81	−0.15[a]	0.22[a]	–	0.22	0.87	
1.1	−0.17	4.50	106.60	−0.05	5.63	63.74	−0.09	0.17	3.32	−0.06	0.11	2.75
1.2	−0.17	4.50	176.64	−0.05	5.62	98.62	−0.09	0.17	5.42	−0.06	0.11	4.85
1.3	−0.17	4.50	235.91	−0.05	5.62	128.19	−0.09	0.17	7.20	−0.06	0.11	6.63
1.4	−0.17	4.50	286.71	−0.05	5.61	153.56	−0.09	0.17	8.72	−0.06	0.11	8.15
1.5	−0.17	4.50	330.74	−0.05	5.61	175.56	−0.09	0.17	10.05	−0.06	0.11	9.47

[a]For the Lognormal distribution, the parameters are: mean and standard deviation.

The geometry of the cross-section is determined by many factors, such as the traffic envelope in combination with the BWR. Additionally, in an SFT, the hydrodynamic loads are directly related to the cross-section's geometry. For example, if the cross-section is enlarged, then the capacity of the SFT will be increased but the effect of these loads will also be larger. Thus, adjusting the cross-section geometry is not a straight forward solution as it might be for traditional structures, like bridges or buildings. However, to increase the structural strength, additional post-tensioning can be added. By varying the physical location of the tendons in the cross-section, the lever arm can be changed. With a larger lever arm the bending capacity will increase.

In Figs. 13 and 14 different tendon layouts and spread angles are presented for the same amount of tendons. By varying the spread angle, different lever arms can be obtained. The most efficient position of asymmetric post-tensioning is as close as possible to the outer fiber. However, post-tension tendons also have to meet construction requirements, such as the intermediate distances between tendons and the ability to actually post-tension. These requirements might conflict with the most efficient location of the tendons. For this case study, a

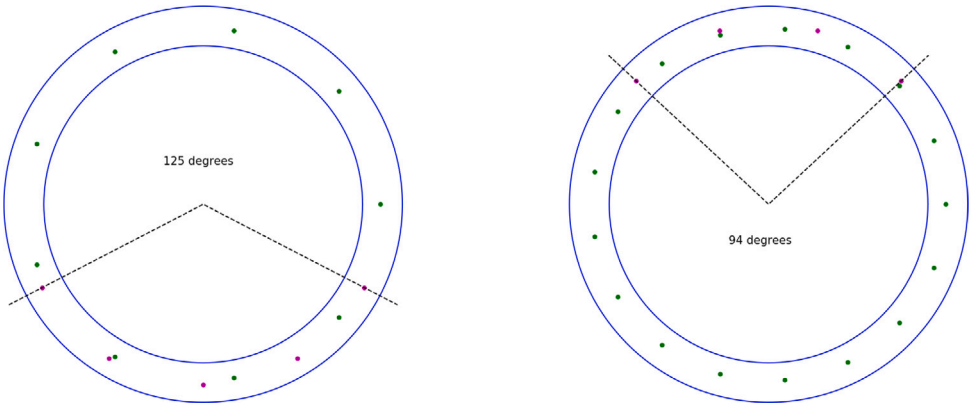

Fig. 16. Layout of the post-tensioning for the cross-section at the center of the spans (left) and at the tether locations (right).

Table 6
Extreme values for $M_{cap,max}$, $V_{cap,max}$, $M_{cap,min}$, $V_{cap,min}$ for different return periods and a BWRs.

BWR	Variable	Return Period & P_F						
		5	10	20	50	100	200	500
		0.2	0.1	0.05	0.02	0.01	0.005	0.002
0	$M_{cap,max}$	43	43	44	44	44	44	44
1.1		128	130	132	134	136	140	142
1.2		198	200	201	204	205	207	208
1.3		257	259	261	262	264	265	266
1.4		308	310	312	313	314	316	319
1.5		352	354	356	358	359	360	364
0	$M_{cap,min}$	55	58	61	66	68	73	76
1.1		97	100	103	106	108	109	111
1.2		133	135	137	140	140	143	147
1.3		161	164	167	169	172	175	178
1.4		187	190	192	195	197	199	204
1.5		209	212	215	217	219	221	223
0	$V_{cap,max}$	2	2	2	2	2	2	2
1.1		4	4	4	4	4	5	5
1.2		6	6	7	7	7	7	7
1.3		8	8	8	8	8	8	8
1.4		10	10	10	10	10	10	10
1.5		11	11	11	11	11	11	11
0	$V_{cap,min}$	2	2	2	2	2	2	2
1.1		3	3	3	3	3	3	3
1.2		5	5	6	6	6	6	6
1.3		7	7	7	7	7	7	7
1.4		9	9	9	9	9	9	9
1.5		10	10	10	10	10	10	10

minimum distance of 1 m from the center to the tendons is considered. Any optimization that can be derived by changing this distance to a minimum value is out of the scope of this paper.

4.3. Reliability analysis

The probability of failure (P_F) of the SFT was tested for bending failure of the SFT tube in the longitudinal direction. Its corresponding limit state is defined by Eq. (7) when $\sigma_f > 0$, from which the bending moments due to traffic ($M_{tr,cap}$) are derived (Section 2.6).

The probability of failure of the SFT under this particular failure mode is defined as $P_F = P(M_{max} > M_{cap,max})$ or $P_F = P(M_{tr,max} > M_{tr,cap,max})$ or equivalent for the minimal moments $P_F = P(M_{min} > M_{cap,min})$ or $P_F = P(M_{tr} < M_{tr,cap,min})$ (Section 2.6). The limit state function is defined in Eq. (11).

$$Z = P(M_{max} > M_{cap,max}) \tag{11}$$

Table 7
Post tension specification and capacity.

Item	Center of span	Tether location
# Axial tendons	9	17
# Asymmetric tendons	5	4
Spread angle [degrees]	125	94
$N_{ax,pt}$ [MN]	−19.2	−36.3
$N_{as,pt}$ [MN]	−10.7	−8.6
a [m]	3.31	−3.75
M_{pt} [MNm]	−35.4	32.1
$M_{cap,max/min} = M_{BWR} + M_{cap,max/min}$ [MNm]	108.4	−141.6
M_{BWR} [MNm]	42.0	−84.0
$M_{tr,cap,max/min}$ [MNm]	66.4	−57.6
$M_{max/min}$ return period [year]	139	439

M_{max} and M_{min} are respectively, the maximum allowable capacity of the SFT at the center of the span and at the tether location (Fig. 6). In other words, it is considered failure when the maximum bending moment exceeds the moment capacity M_{cap}. These limit values are directly depending on the asymmetric post-tensioning.

The reliability analysis is divided into two parts. First, the resulting daily bending moments and shear forces obtained from the structural model are fitted to probability distribution functions. From which their corresponding annual maximum frequency curves are derived. The second part is defined by the design of the post-tensioning. For a given SFT design, the limit bending moments are found. Consequently, the probabilities of exceeding these limit values are found through the annual maximum frequency curves.

The structural analysis was performed for different buoyancy-weight ratio (BWR) values ranging from 1.1 to 1.5. In this paper, the authors are focused on a BWR = 1.1 and the corresponding $M_{cap,max}$ and $M_{cap,min}$ to determine the probability of failure of the SFT. From a design point view a BWR close to 1.0 is most economical. The BWR ratio results in a distributed load. By application of a lower BWR, the spans used in the structure can be larger. If larger spans can be used, less supporting pontoons are needed. The authors realize that other elements, such as loading or stability requirements, might cause the need for a larger BWR, but these are considered to be beyond the scope of this paper. Nevertheless, the results for other BWR values as well as their associated $M_{cap,max}$, $M_{cap,min}$, $V_{cap,max}$ and $V_{cap,min}$ are also shown.

4.3.1. Frequency curves

The resulting daily values of bending moments ($M_{cap,max}$&$M_{cap,min}$) and shear forces ($V_{cap,max}$&$V_{cap,min}$) obtained from the structural model (Section 4.2) were fitted to probability distribution functions. The results are shown in Table 4.

Table B.1
Vehicle categories of WIM observations.

Item	Class	Code											
1	B2	B11	B2										
2	B3	B111	B12	B3									
3	O3	O3											
4	O4	O4											
5	O5	O5											
6	O6	O6											
7	O8	O8											
8	O9	O9											
9	O10	O=											
10	O11	O>											
11	R5	R11111	R1112	R1211	R122								
12	R6	R111111 R1212	R11112 R123	R11121 R1311	R1113 R132	R11211	R1122	R12111					
13	R7	R1111111 R124 R1132 R11212	R111112 R13111 R115 R11221	R111121 R133 R121111	R11113 R2221 R12112	R111211 R223 R1213	R11122 R11311 R12211	R112111 R1123 R1222					
14	R8	R11111111 R11213 R121211 R13211	R1111112 R112211 R12122 R1322	R1111121 R11222 R1214 R134	R111113 R1124 R122111 R2123	R111122 R113111 R12212 R2213	R1112111 R11312 R12221 R2222	R111212 R11321 R1223 R224	R111221 R1133 R12311	R11123 R1211111 R1232	R1121111 R121112 R125	R112112 R121121 R131111	R112121 R12113 R1313
15	R9	R1112121 R1211121 R12321 R2214	R1112211 R121113 R1233 R2223	R11124 R1212111 R126 R225	R1121121 R121212 R1314 R234	R112113 R121221 R132111 R3312	R1122111 R12123 R13221 R54	R112221 R1221111 R1323	R11223 R122112 R1332	R1125 R122121 R1341	R1134 R12213 R135	R12111111 R1224 R1413	R1211112 R123111 R144
16	T3	T11O1											
17	T4	T111O1	T11O11	T11O2	T12O1	T21O1	T2O2						
18	T5	T111O11 T12O11	T111O2 T12O2	T11O111 T21O11	T11O12 T21O2	T11O21 T2O21	T11O3 T2O3	T3O2					
19	T6	T111O111 T12O111	T111O12 T12O12	T111O21 T12O21	T111O3 T12O3	T11O1111 T21O111	T11O112 T21O12	T11O121 T21O21	T11O13 T21O3	T11O211 T2O22	T11O22 T2O4	T11O31 T3O3	T11O4
20	T7	T111O112 T12O31	T111O121 T12O4	T111O13 T21O211	T111O22 T21O22	T111O31 T21O4	T111O4 T3O4	T12O1111	T12O112	T12O121	T12O13	T12O211	T12O22
21	V2	V11											
22	V3	V111	V11A1	V12	V21	V3							
23	V4	V1111	V112	V11A11	V11A2	V121	V13	V211	V22	V4			
24	V5	V111A11	V111A2	V11A111	V11A12	V12A11	V12A2	V21A11	V21A2				
25	V6	V1111A11 V13A2	V1111A2 V211A11	V111A111 V211A2	V111A12 V21A12	V112A11 V22A11	V112A2 V22A2	V121A11	V12A111	V12A12	V12A21	V12A3	V13A11
26	V7	V1111A111 V13A21	V1111A12 V13A3	V1111A3 V211A12	V112A111 V211A3	V112A12 V22A111	V112A21 V22A12	V112A3 V22A21	V121A111 V22A3	V121A12 V4A12	V121A3	V13A111	V13A12

The criteria for selecting an appropriate probability distribution function was made based on maximum likelihood estimation (MLE) and by visual inspection. Table 5 presents the parameters of the fitted distributions.

The corresponding annual maxima frequency curves for both the bending moments and shear forces for a BWR of 1.1 are shown in Fig. 15. From these plots is possible to determine the return period (or probability of exceedance) of particular values for bending moments and shear forces. The corresponding $M_{cap,max}$, $M_{cap,min}$, $V_{cap,max}$, and $V_{cap,min}$ values for different return periods (or probability of exceedance) and BWR magnitudes are depicted in Table 6. The results appear to be sensitive to the choice of BWR. As the BWR increases, the values for both the maximum bending moments and maximum shear forces also increases. This highlights the importance of the choice of BWR when designing an SFT.

4.3.2. Post-tensioning design

Post-tensioning is expensive in monetary terms. Thus, an economical design should limit the amount of post-tensioning. With the methodology presented in this paper, the maximum moment due to traffic ($M_{tr,max,min}$) can be found more accurately and the design can therefore be economically optimized. The probability of occurrence associated with the resulting $M_{cap,min,max}$ is obtained from the frequency curves derived from Section 4.3.1. Thus, the probability of exceeding the limit values is translated as the probability of failure of the SFT.

In Fig. 16 the location of post-tension tendons is presented for both the section at the center of the span and at the tether location. The proposed design layout is presented in Table 7 and the capacity for the maximum moment due to traffic is derived. According to Fig. 15(a) and Table 6, the resulting M_{cap} at the center of span and at the tether location have a return period of 139 ($P_F = 0.01$) and 439 ($P_F = 0.005$) years respectively.

The post-tensioning design can be modified to fit any probability of exceedance (or return period), specified by the target reliability index, presented in Fig. 15(a) and Table 6. In this paper, the presented layout is used as an example to show the application of the methodology.

5. Discussion

The inter-vehicle model methodology presented in this paper combines uni-variate and multi-variate models (copulas). This not only allows the simulation of the inter-vehicle distance but also models the

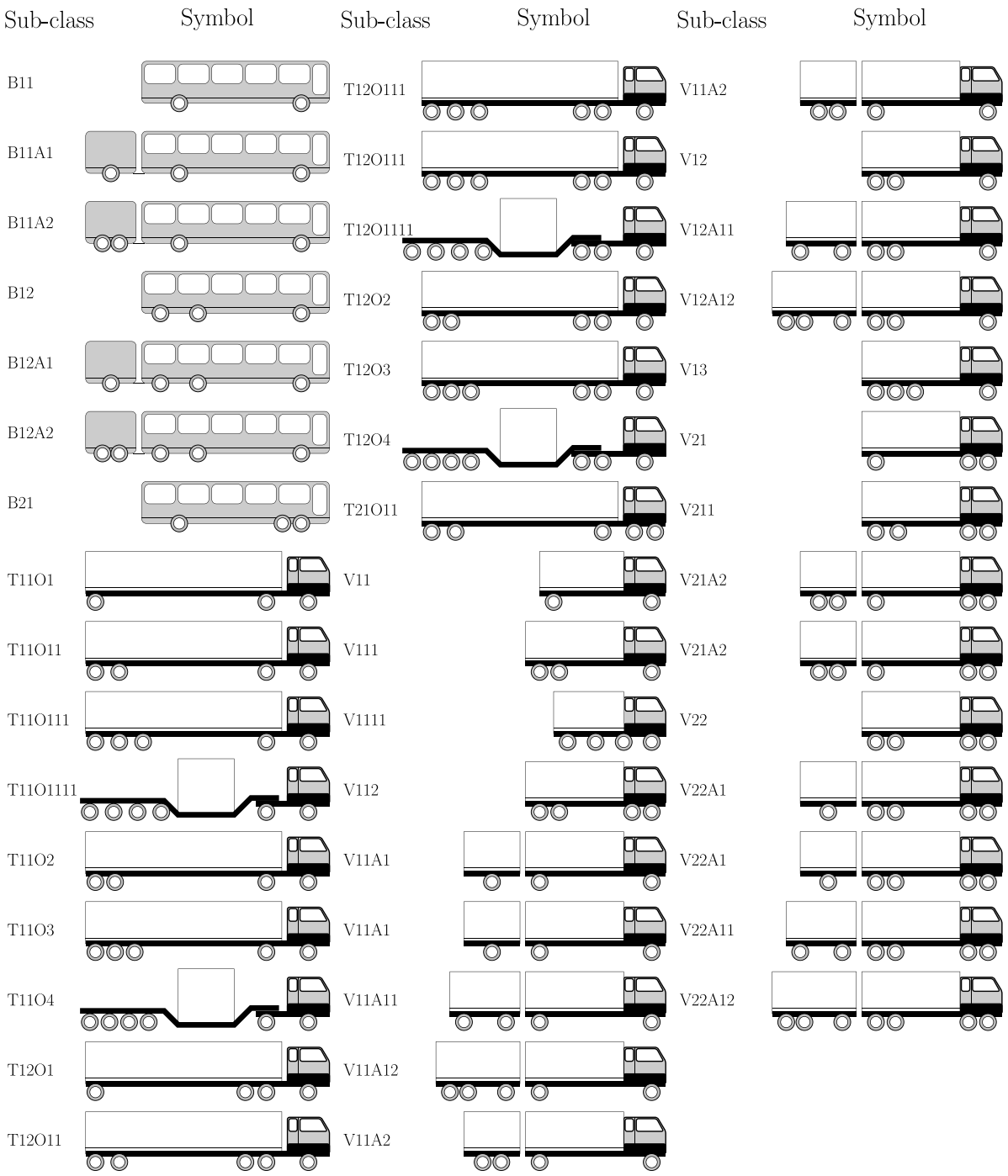

Fig. B.1. WIM Vehicle indexing [33].

number of vehicles per lane per day and their classification according to the different vehicle categories (Appendix B). Each vehicle category is defined by their axle weight and inter-axle distance. The selection of each one of the passing vehicles is random. In this way, it is possible to obtain a "train" of vehicles that is closer to reality. One of the main advantages of this model is its flexibility. The model can be used for any number of vehicle categories, lanes and traffic scenarios. In this case study, the model was developed on basis of one single "ideal day", nevertheless, the inter-vehicle model can be extended to encompass specific daily conditions (weekends and holidays) or seasonal conditions.

In the setup presented in this article, the geometry of the cross-section and the span length are arbitrary choices. Larger BWR values lead to higher bending moments and shear forces as shown in Table 6. This can influence other design decisions such as shorter spans or larger tether sections that could affect the stability of the system. In this paper, the resulting bending moments and shear forces were computed for different BWR values. However, a BWR of 1.1 was chosen for further analysis. In any case, a design should be optimized for different circumstances. Possibilities to consider are (but not limited to):

- Using larger BWR values. This will lead to larger bending moments and shear forces. Consequently, other requirements for

Table C.1
Daily proportion of vehicles' categories. 10th April 2013.

Vehicle category	C_L2	F_L2_A	F_L2_B	C_L3	F_L3_A	F_L3_B
B2	0.61	5.56	1.65	0.69	0.58	0.39
B3	1.83	0.00	3.31	0.61	0.17	0.33
O3	3.05	1.85	2.13	0.69	0.42	1.11
O4	15.24	3.70	4.96	4.59	1.83	2.66
O5	0.61	1.85	0.71	0.61	0.58	0.20
O8	0.00	0.00	0.00	0.17	0.25	0.09
O9	0.00	0.00	0.00	0.00	0.08	0.00
OT10	0.00	0.00	0.00	0.00	0.00	0.02
OT11	0.00	0.00	0.00	0.00	0.00	0.00
R5	0.00	0.00	0.00	0.00	0.00	0.07
R6	0.00	0.00	0.00	0.17	0.83	0.11
R7	0.00	0.00	0.24	0.26	0.42	0.30
R8	0.00	0.00	0.00	0.26	0.17	0.41
R9	0.00	0.00	0.00	0.09	0.08	0.07
T3	1.83	3.70	2.60	5.37	4.33	4.22
T4	10.98	16.67	14.89	15.34	19.83	18.35
T5	26.83	33.33	37.12	29.29	38.25	36.04
T6	2.44	7.41	2.60	6.07	6.25	6.81
T7	0.61	0.00	0.00	0.26	0.33	0.33
V2	14.63	9.26	15.37	14.99	9.92	12.80
V3	3.66	1.85	1.65	4.51	1.92	4.16
V4	14.02	5.56	5.91	8.23	6.67	6.03
V5	1.83	5.56	4.73	5.37	5.33	3.53
V6	1.22	3.70	1.89	1.65	1.67	1.61
V7	0.61	0.00	0.24	0.61	0.08	0.37

Table D.2
Monthly proportion of vehicles' categories. April 2013.

Vehicle category	Proportion [%]
B2	1.014
B3	0.779
O3	1.295
O4	3.116
O5	0.400
O8	0.128
O9	0.026
OT10	0.012
OT11	0.006
R5	0.047
R6	0.216
R7	0.264
R8	0.317
R9	0.054
T3	3.851
T4	17.795
T5	35.481
T6	5.871
T7	0.277
V2	12.801
V3	3.582
V4	6.902
V5	4.005
V6	1.445
V7	0.297

Table E.1
Copula fit for inter-vehicle distances per traffic type. April 2013.

Day	C_L2	C_L3	F_L2_A	F_L3_A	F_L2_B	F_L3_B
4	Joe	Frank	Joe	BB8	Joe	BB8
5	Gaussian	Gaussian	Clayton	Frank	Joe	Joe
6	t	Frank	Joe	t	Joe	Joe
7	Frank	Frank	Joe	Frank	Joe	BB7
8	Joe	Clayton	Clayton	Clayton	Gaussian	Gumbel
10	Gumbel	Frank	Joe	BB8	Joe	BB7
11	Gaussian	Frank	Joe	BB8	Joe	Joe
12	Gaussian	Joe	Joe	t	Joe	Joe
13	Clayton	Frank	t	BB8	Joe	Joe
14	t	Frank	Joe	Gaussian	Joe	Joe
15	t	Frank	Gaussian	Clayton	Joe	Joe
17	Gaussian	Gaussian	Joe	BB8	Gumbel	BB8
18	Gumbel	Frank	Joe	Frank	Joe	BB8
19	Frank	Frank	t	Clayton	Joe	Joe
20	Gaussian	Frank	Joe	t	Joe	Joe
21	BB7	Frank	BB7	Frank	Joe	BB8
22	t	Clayton	Clayton	Gaussian	Joe	Joe
24	Gaussian	Gaussian	t	BB8	Joe	Joe
25	Gaussian	Clayton	Joe	BB8	Joe	BB8
26	Joe	t	Gaussian	BB8	Joe	BB8
27	t	Frank	Gumbel	BB8	Joe	BB8
28	Joe	Frank	Joe	BB8	Joe	BB8
29	Gaussian	Clayton	Gaussian	Frank	Joe	BB7

pontoons, tether systems and foundations will be affected. However, a higher BWR could contribute to the stability of the system. Moreover, a longitudinal variation of the BWR might be applicable depending on local situations or specific design.

- In this paper, a monolithic structure is considered. However, a more flexible structure with longitudinal rotational springs could be of interest depending on local circumstances such as the action of hydrodynamic loads. This will help avoid local peak stresses or cross-section results. Yet, leakage at a flexible joint can be challenging from a design point of view.
- If tendons with larger diameter are used in combination with a smaller spread angle, mixed diameters of post-tensioning tendons for both axial and asymmetric layout can be beneficial for the lever arm.
- In this paper, the tendons are considered to be straight. It is a possibility to apply curved tendons in the longitudinal direction to benefit from the counterbalancing force provided by this curvature. However, curved tendons will generate an additional load in the radial direction.
- Although the SFT design presented in this paper consists of a single tubular tube, the proposed methodology is applicable to different designs of SFT (double tubes or different cross-section geometries as presented in [35]).

6. Conclusions

In this paper, a methodology to study the reliability of a pontoon-type SFT is presented. Considering that this structure has not been built yet, it is important that the variables of interest are characterized as close to reality as possible. For the purpose of this paper, traffic loading is the variable of interest. The methodology is divided into two main parts, (i) simulation of traffic using a copula-based model, and (ii) a structural model to test the SFT for a given failure mechanism (leakage due to bending of the SFT tube in the longitudinal direction). Finally, the reliability of the structure is investigated under the aforementioned failure mechanism.

From the original data set (WIM), several characteristics were extracted. Namely, (i) the inter-vehicle distance, (ii) the daily proportion of vehicles per lane, per category and per traffic type, and (iii) the monthly proportion of vehicles. The first is used as input for the copula-based model, the second is used to create and "ideal" traffic day, and the third is used to create a large data set of vehicles per category. All of these were combined to finally simulate traffic flowing through the SFT.

The results from the copula-model showed that the selected copulas can to capture the inter-vehicle distance. Although the correlation of the inter-vehicle distance from the WIM data set is relatively small, the probabilistic model provides a great advantage since with just over a month of measurements it was possible to simulate a total of 1 year of data. However, longer data sets can be produced. The combination of the inter-vehicle copula-model and random sampling from the VH data set (which provides the vehicle's characteristics) resulted in one vector that characterizes daily traffic at the SFT. This vector was used as input for the structural model.

Table E.2
Spearman's correlation coefficient for observations and simulations for inter-vehicle distance. April 2013.

Day	C_L2		C_L3		F_L2_A		F_L3_A		F_L2_B		F_L3_B	
	Obs.	Sim.	Obs.	Sim.	Obs.	Sim.	Obs.	Sim.	Obs.	Sim.	Obs.	Sim.
4	0.213	0.091	−0.039	−0.088	0.477	0.584	0.218	0.300	0.149	0.177	0.088	0.113
5	0.084	0.259	−0.010	−0.017	0.535	0.563	0.177	0.170	0.109	0.129	0.097	0.140
6	0.068	−0.014	−0.103	−0.088	0.153	0.312	0.157	0.156	0.140	0.208	0.089	0.186
7	−0.045	0.004	−0.121	−0.160	0.508	0.163	0.265	0.240	0.152	0.186	0.136	0.173
8	0.099	0.231	0.033	−0.022	0.500	0.350	0.116	0.172	0.210	0.060	0.179	0.177
10	0.114	0.048	−0.050	−0.038	0.154	0.857	0.281	0.256	0.131	0.188	0.117	0.171
11	−0.003	−0.037	−0.023	0.007	0.106	0.367	0.245	0.242	0.162	0.218	0.102	0.112
12	−0.021	−0.142	0.004	−0.031	0.486	0.097	0.222	0.177	0.054	0.069	0.090	0.150
13	0.036	0.040	−0.029	−0.046	0.202	0.398	0.245	0.313	0.112	0.294	0.104	0.110
14	0.124	0.303	−0.035	0.023	0.414	0.419	0.190	0.227	0.147	0.226	0.118	0.147
15	−0.333	−0.103	0.065	0.003	0.300	0.400	0.115	0.176	0.154	0.078	0.119	0.165
17	0.133	0.170	−0.019	−0.043	0.365	0.351	0.289	0.290	0.156	0.132	0.099	0.138
18	0.154	0.100	−0.054	−0.068	0.388	−0.159	0.177	0.129	0.086	0.165	0.085	0.114
19	0.259	0.184	−0.086	−0.116	0.060	0.414	0.216	0.222	0.211	0.323	0.086	0.096
20	−0.001	−0.008	−0.009	0.017	0.566	0.712	0.165	0.100	0.121	0.152	0.101	0.136
21	0.148	0.262	−0.093	−0.088	0.307	0.384	0.231	0.256	0.204	0.270	0.086	0.122
22	−0.355	−0.346	0.036	0.079	0.164	0.291	0.059	0.112	0.197	0.067	0.112	0.152
24	0.103	0.107	0.001	−0.045	0.102	−0.278	0.168	0.176	0.106	0.146	0.067	0.123
25	0.115	0.125	0.007	0.059	0.389	0.218	0.139	0.068	0.217	0.296	0.122	0.155
26	0.088	0.007	−0.044	−0.067	0.470	0.517	0.256	0.277	0.161	0.228	0.091	0.150
27	−0.049	−0.147	−0.006	0.013	0.535	0.348	0.284	0.288	0.105	0.220	0.113	0.148
28	0.002	−0.108	−0.055	−0.025	0.558	0.593	0.222	0.240	0.066	0.120	0.092	0.155
29	−0.257	−0.388	0.023	0.047	0.543	0.257	0.053	0.100	0.274	0.325	0.158	0.125

To simulate the structure's response over long periods of time, the proposed structural modeling approach needs to be as efficient as possible. Thus, by defining the global DSM (Direct Stiffness method) approach with long beams and a dedicated DEM approach for intermediate loading, the FEM model became as efficient as possible to avoid lag in the analysis. The analysis time was further reduced by applying the superposition principle.

Results from the structural model provided the maximum and minimum bending moments and shear forces under the traffic loading for different BWR values. From these results, the annual distribution of these variables was obtained and, consequently, their extreme values for several return periods.

Finally, the values of M_{cap} at the center of the span and at the tether location were obtained. These values define the limit state function for failure due to bending of the tube in the longitudinal direction (Section 4.3). In other words, failure could only occur if the resulting bending moments are larger than M_{cap}. The return periods for both M_{cap} of 108.4 MNm and −141.6 MNm, are 139 and 439 years at the center of the span and tether location respectively. Their corresponding probabilities of failure are 0.01 and 0.005. These probabilities can be considered as very high when compared to international safety standards. For example, a structure with a RC3 reliability level ($\beta = 4.3$) has an estimated probability of failure equal to 8.5e−06 [9] assuming that the lifetime of the structure is 50 years. For the case of an SFT, the consequences of failure are much more severe compared to regular buildings. For this reason, M_{cap} with larger return periods are needed. In such case, changing the number and location of the tendons or using a different BWR (Section 5) could be appropriate.

Due to the lack of data regarding the structural response of an SFT, the combination of probabilistic modeling with structural analysis offers the possibility to study the design choices of this structure. This paper shows an effective way to combine probabilistic modeling through copulas and structural analysis to simulate the traffic loads passing through the SFT and their effect on the structure. This methodology offers great flexibility because it can be used to test the reliability of the SFT considering other loading variables. For example, external environmental variables such as waves, currents, and their simultaneous action on an SFT. Moreover, this methodology is not restricted to be used only on an SFT. It can be applied to other civil structures where the data is scarce.

7. Recommendations

The results showed to be sensitive to the choice of BWR, therefore, this choice should be handled with caution when designing an SFT. Other limit states should be considered to assess the reliability of an SFT. For example, failure of the tethers, at the foundation or the cross-section. These failure modes could be considered as stand-alone limit states or in combination with each other. Assessment of combined failure modes could be executed through Bayesian networks.

CRediT authorship contribution statement

G.A. Torres-Alves: Designed the model and the computational framework, Analysed the data, Statistical calculations, Structural analysis, Writing – original draft. **C.M.P. 't Hart:** Designed the model and the computational framework, Analysed the data, Structural analysis, Writing – original draft. **O. Morales-Nápoles:** Resources, Reviewed the manuscript. **S.N. Jonkman:** Resources, Reviewed the manuscript.

Declaration of competing interest

The authors declare that they have no known competing financial interests or personal relationships that could have appeared to influence the work reported in this paper.

Acknowledgments

This research was supported by the Submerged Floating Tunnel (SFT) Team. This research project is commissioned by the Chinese engineering and construction company China Communications Construction Co., Ltd. (CCCC) and is jointly carried out by 8 institutions of universities, scientific research institutes, engineering consulting firms, design and construction companies. The authors would like to thank the Ministry of Infrastructure and Water Management and TNO for their permission to use the traffic data of April 2013.

Appendix A. Traffic simulation algorithm

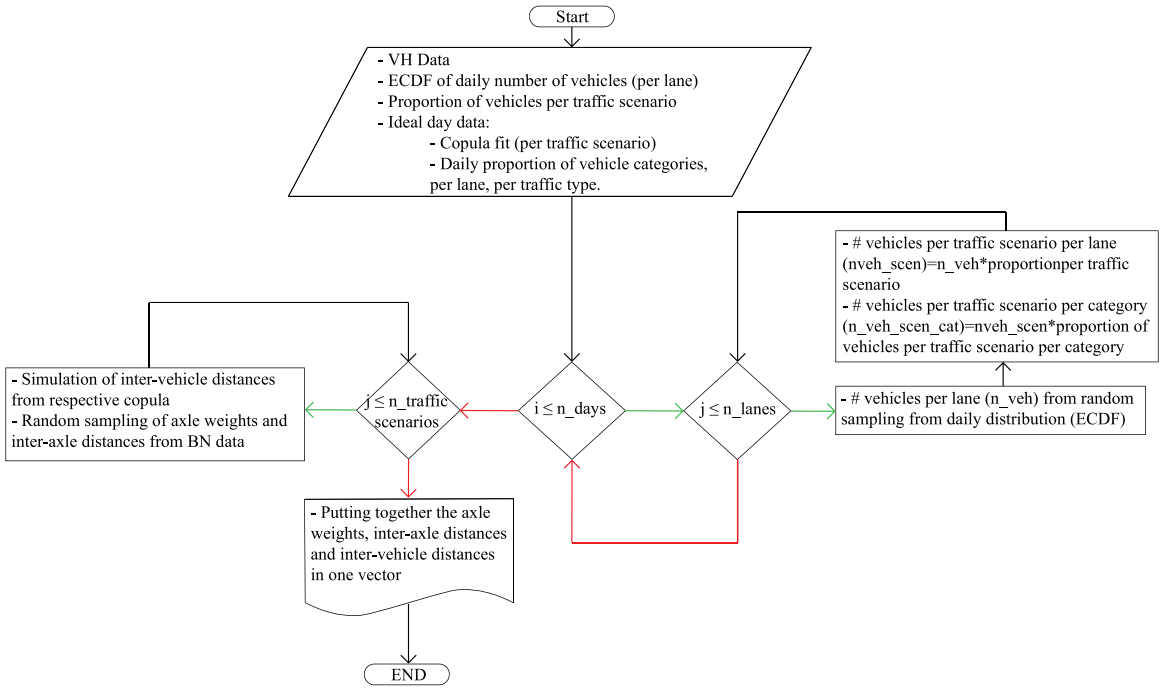

Appendix B. Vehicle categories

See Table B.1 and Fig. B.1.

Appendix C. Daily proportion of vehicles' categories

See Table C.1.

Appendix D. Monthly proportion of vehicles' categories. April 2013.

See Table D.2.

Appendix E. Copula results—april 2013

See Tables E.1 and E.2.

References

[1] Mazzolani FM, Faggiano B, Martire G. Design aspects of the AB prototype in the Qiandao Lake. Procedia Eng 2010;4:21–33. http://dx.doi.org/10.1016/j.proeng.2010.08.005.

[2] Martire G. The development of submerged floating tunnels as an innovative solution for waterway crossings (Ph.D. thesis), Università degli Studi di Napoli Federico II; 2010, p. 316. http://dx.doi.org/10.6092/UNINA/FEDOA/8407.

[3] Shengzhong W, Xiang C, Qinxi L, Gengren C. Research on type selection of submerged floating tunnel of qiongzhou strait. Procedia Eng 2016;166:307–16. http://dx.doi.org/10.1016/j.proeng.2016.11.553.

[4] Lunniss R, Baber J. Immersed tunnels. Taylor & Francis; 2013, URL https://books.google.nl/books?id=dUBaw8fQRAMC.

[5] Tveit P. Submerged floating tunnels (SFTs) for Norwegian fjords. Procedia Eng 2010;4:135–43. http://dx.doi.org/10.1016/j.proeng.2010.08.016, ISAB-2010. URL http://www.sciencedirect.com/science/article/pii/S1877705810005138.

[6] Grantz P.E. WC. Conceptual study for a deep water, long span, submerged floating tunnel (SFT) crossing. Procedia Eng 2010;4:61–70. http://dx.doi.org/10.1016/j.proeng.2010.08.008, ISAB-2010. URL http://www.sciencedirect.com/science/article/pii/S1877705810005059.

[7] Fédération internationale du béton. Guidelines for submerged floating tube bridges - FIB BULLETIN NO. 96. CEB-Fib; 2020, URL http://dx.doi.org/10.35789/fib.BULL.0096.

[8] Ingerslev C. Immersed and floating tunnels. Procedia Eng 2010;4:51–9. http://dx.doi.org/10.1016/j.proeng.2010.08.007.

[9] European Committee for Standardization. EN 1990. Eurocode: Basis of structural design. Brussels: CEN; 2002.

[10] American Association of State Highway and Transportation Officials. LRFD road tunnel design and construction guide specifications. American Association of State Highway and Transportation Officials; 2017.

[11] Ghasemi SH, Nowak A. Reliability analysis of circular tunnel with consideration of the strength limit state. Geomech Eng 2018;15:433–9. http://dx.doi.org/10.12989/gae.2018.15.3.879.

[12] Azadi M, Ghasemi SH, Mohammadi M. Reliability analysis of tunnels with consideration of the earthquakes extreme events. Geomech Eng 2020;22:433–9. http://dx.doi.org/10.12989/gae.2020.22.5.433.

[13] ISO 2394. General principles on reliability for structures, Vol. 2015. 2015.

[14] JCSS. JCSS probabilistic model code. 2001.

[15] Baravalle M, Köhler J. A risk-based approach for calibration of design codes. Struct Saf 2019;78(September 2017):63–75. http://dx.doi.org/10.1016/j.strusafe.2018.12.003.

[16] Baravalle M, Köhler J. Risk and reliability based calibration of design codes for submerged floating tunnels. Procedia Eng 2016;166(1877):247–54. http://dx.doi.org/10.1016/j.proeng.2016.11.547.

[17] Mendoza-Lugo MA, Delgado-Hernández DJ, Morales-Nápoles O. Reliability analysis of reinforced concrete vehicle bridges columns using non-parametric Bayesian networks. Eng Struct 2019;188:178–87. http://dx.doi.org/10.1016/j.engstruct.2019.03.011, URL http://www.sciencedirect.com/science/article/pii/S014102961833565X.

[18] Tabatabai H, Titi H, Zhao J. WIM-based assessment of load effects on bridges due to various classes of heavy trucks. Eng Struct 2017;140:189–98. http://dx.doi.org/10.1016/j.engstruct.2017.02.060, URL https://www.sciencedirect.com/science/article/pii/S0141029616312731.

[19] Spissu E, Pinjari A, Pendyala R, Bhat C. A copula-based joint multinomial discrete-continuous model of vehicle type choice and miles of travel. Transportation 2009;36(4):403–22. http://dx.doi.org/10.1007/s11116-009-9208-x, Copyright: Copyright 2009 Elsevier B.V., All rights reserved.

[20] Bhat CR, Eluru N. A copula-based approach to accommodate residential self-selection effects in travel behavior modeling. Transp Res B 2009;43(7):749–65. http://dx.doi.org/10.1016/j.trb.2009.02.001, URL http://www.sciencedirect.com/science/article/pii/S0191261509000204.

[21] Zou Y, Zhang Y. A copula-based approach to accommodate the dependence among microscopic traffic variables. Transp Res C 2016;70:53–68. http://dx.doi.org/10.1016/j.trc.2015.11.003, URL http://www.sciencedirect.com/science/article/pii/S0968090X15003940.

[22] Gong C, Frangopol DM. Reliability of steel girder bridges with dependent corrosion growth. Eng Struct 2020;224:111125. http://dx.doi.org/10.1016/j.engstruct.2020.111125, URL https://www.sciencedirect.com/science/article/pii/S0141029619335023.

[23] Fu X, Li H-N, Li G, Dong Z-Q, Zhao M. Failure analysis of a transmission line considering the joint probability distribution of wind speed and rain intensity. Eng Struct 2021;233:111913. http://dx.doi.org/10.1016/j.engstruct.2021.111913, URL https://www.sciencedirect.com/science/article/pii/S0141029621000638.

[24] wei Wang Z, ming Zhang W, min Tian G, Liu Z. Joint values determination of wind and temperature actions on long-span bridges: Copula-based analysis using long-term meteorological data. Eng Struct 2020;219:110866. http://dx.doi.org/10.1016/j.engstruct.2020.110866, URL https://www.sciencedirect.com/science/article/pii/S014102961935357X.

[25] Torres-Alves GA, Morales-Nápoles O. Reliability analysis of flood defenses: The case of the Nezahualcoyotl dike in the aztec city of Tenochtitlan. Reliab Eng Syst Saf 2020;203:107057. http://dx.doi.org/10.1016/j.ress.2020.107057, URL http://www.sciencedirect.com/science/article/pii/S0951832020305585.

[26] Sklar A. Fonctions de répartition à n dimensions et leurs marges. Publ Inst Stat Univ Paris 1959;8:229–31.

[27] Joe H. Dependence modeling with copulas. Chapman and Hall/CRC; 2014, http://dx.doi.org/10.1201/b17116.

[28] Schepsmeier, Stöber, Brechmann, Gräler, Nagler, Erhardt. VineCopula: statistical inference of vine copulas. 2018, https://cran.r-project.org/web/packages/VineCopula/index.html.

[29] R Core Team. R: A language and environment for statistical computing. Vienna, Austria: R Foundation for Statistical Computing; 2020, URL https://www.R-project.org/.

[30] Morales-Nápoles O, Steenbergen RD. Analysis of axle and vehicle load properties through Bayesian Networks based on Weigh-in-Motion data. Reliab Eng Syst Saf 2014;125:153–64. http://dx.doi.org/10.1016/j.ress.2014.01.018, Special issue of selected articles from ESREL 2012. URL http://www.sciencedirect.com/science/article/pii/S0951832014000283.

[31] Morales-Nápoles O, Steenbergen RDJM. Large-scale hybrid Bayesian network for traffic load modeling from weigh-in-motion system data. J Bridge Eng 2015;20(1):04014059. http://dx.doi.org/10.1061/(ASCE)BE.1943-5592.0000636, arXiv:https://ascelibrary.org/doi/pdf/10.1061/%28ASCE%29BE.1943-5592.0000636. URL https://ascelibrary.org/doi/abs/10.1061/%28ASCE%29BE.1943-5592.0000636.

[32] EN1992 Part 3 for Standardization, European Committee. EN1992 Part 3: Liquid retaining and containing structures. CEN; 2006.

[33] Vervuurt A, Pruiksma J, Steenbergen R, Courage W, Miraglia S, (TUD) OMN. Statische belastingen Herijking verkeersbelastingen voor brugconstructies op basis van WIM analyses van april 2013 (IQ-2014-33c). Report, TNO; 2015.

[34] Mendoza-Lugo MA, Morales-Napoles O, Delgado-Hernandez DJ. A non-parametric Bayesian network for multivariate probabilistic modelling of weigh-in-motion system data. 2021, unpublished.

[35] Nestegård A, Haugerud S, Solemsli J, Engebretsen K, Wåsjø K, Myhr A. K3- K4 Design basis report - Bjornafjord submerged floating tunnel. Technical report, Norconsult; 2016.